

# Cooperative Tracking of Cyclists Based on Smart Devices and Infrastructure

Günther Reitberger, Stefan Zernetsch, Maarten Bieshaar, Bernhard Sick, Konrad Doll, and Erich Fuchs

**Abstract**—In future traffic scenarios, vehicles and other traffic participants will be interconnected and equipped with various types of sensors, allowing for cooperation based on data or information exchange. This article presents an approach to cooperative tracking of cyclists using smart devices and infrastructure-based sensors. A smart device is carried by the cyclists and an intersection is equipped with a wide angle stereo camera system. Two tracking models are presented and compared. The first model is based on the stereo camera system detections only, whereas the second model cooperatively combines the camera based detections with velocity and yaw rate data provided by the smart device. Our aim is to overcome limitations of tracking approaches based on single data sources. We show in numerical evaluations on scenes where cyclists are starting or turning right that the cooperation leads to an improvement in both the ability to keep track of a cyclist and the accuracy of the track particularly when it comes to occlusions in the visual system. We, therefore, contribute to the safety of vulnerable road users in future traffic.

## I. INTRODUCTION

### A. Motivation

In our work, we envision a future mixed traffic scenario [1] where traffic participants, such as automated driving cars, trucks, and intelligent infrastructure equipped with sensors, electronic maps, and Internet connection, share the road with vulnerable road users (VRUs), such as pedestrians and cyclists, equipped with smart devices. Each of them itself determines and continuously maintains a local model of the surrounding traffic situation. This model does not only contain information by each traffic participant's own sensory perception, but is the result of cooperation with other traffic participants and infrastructure in the local environment, e.g., based on vehicular ad hoc networks. This joint knowledge is exploited in various ways, e.g., to increase the perceptual horizon of individual road users beyond their own sensory capabilities. Although modern vehicles possess many forward looking safety systems based on various sensors, still dangerous situations for VRUs can occur as a result of occlusions or sensor malfunctions. Cooperation between the different road users can resolve occlusion situations and improve the overall performance regarding measurement accuracy, e.g., precise positioning.

G. Reitberger and E. Fuchs are with the FORWISS, University of Passau, Passau, Germany [reitberg@forwiss.uni-passau.de](mailto:reitberg@forwiss.uni-passau.de), [fuchse@forwiss.uni-passau.de](mailto:fuchse@forwiss.uni-passau.de)

M. Bieshaar and B. Sick are with the Intelligent Embedded Systems Lab, University of Kassel, Kassel, Germany [mbieshaar@uni-kassel.de](mailto:mbieshaar@uni-kassel.de), [bsick@uni-kassel.de](mailto:bsick@uni-kassel.de)

S. Zernetsch and K. Doll are with the Faculty of Engineering, University of Applied Sciences Aschaffenburg, Aschaffenburg, Germany [stefan.zernetsch@h-ab.de](mailto:stefan.zernetsch@h-ab.de), [konrad.doll@h-ab.de](mailto:konrad.doll@h-ab.de)

In this article we propose a cooperative approach to track cyclists at an urban intersection robustly and accurately. The cooperatively obtained positional information can then subsequently be used for intention detection [2]. In contrast to bare data fusion, cooperation also captures the interactions between different participants. Therefore, we use cooperation as an umbrella term including fusion as an integral part.

### B. Main Contributions and Outline

The main contribution of this article is an approach to cooperatively detect and track the position of cyclists at an urban intersection. The proposed method incorporates positional information originating from the camera tracks of the cyclist's head trajectory as well as velocity and yaw rate estimates originating from a smart device carried by the cyclist. This information is adaptively combined using an extended Kalman filtering approach. The resulting cooperative tracking mechanism is accurate and, furthermore, it can cope with short term occlusion. The novel metric MOTAP is introduced to evaluate the benefit of cooperation in comparison to a single entity approach.

The remainder of this article is structured as follows: In Sec. II, the related work in the field of cooperative transportation and tracking methods including smart devices is reviewed. Sec. III describes the overall approach to cooperatively track cyclists. The methods and metrics used for evaluation are described in Sec. IV. In Sec. V, the experimental results are presented. Finally, in Sec. VI the main conclusions and the open challenges for future work are discussed.

## II. RELATED WORK

Many dangerous situations involving vehicles and VRUs occur in urban areas. The German project Ko-PER of the Ko-FAS research initiative [3] aims to increase the road safety by combining infrastructure-based perception enriched with data from vehicles enabling cooperative perception.

In [4], Thielen et al. presented a prototype system incorporating a vehicle with the ability of C2X communication and a cyclist with a WiFi enabled smartphone. The authors were able to successfully test a prototype application that warns a vehicle driver if the collision with a crossing cyclist is likely to occur within the next 5 seconds. A similar prototype system including Car2Pedestrian communication was proposed by Engel et. al. in [5]. However, the tracking of the VRU is limited by its positional accuracy due to the usage of smartphone sensors only. It does not make use of a cooperative tracking mechanism. Another approach,

combining a radar equipped infrastructure and smart devices in a cooperative way is described by Ruß et. al. in [6]. The radar information is used to correct the GNSS position data of the smartphone using a simple combination mechanism with fixed weights. Besides a prototype system, the authors did not provide a quantitative evaluation. In [7], Merdrignac et. al. propose a cooperative VRU protection system in which vehicles and pedestrians exchange vehicle to pedestrian messages (V2P) about their position successfully resolving occlusion, i.e., non-line of sight situations. Their proposed system is limited in the real world application due to the necessity of precise smart device localization capabilities, which cannot be provided by the built-in GPS.

In [1], we presented a cooperative, holistic concept to detect intentions of VRUs by means of collective intelligence, including smart devices carried by the VRU itself. We proposed an approach to cooperatively detect cyclists' starting motion and to forecast their future trajectory in [2]. The approach was limited in its application due to the requirement of precise positional information for the trajectory forecast. Particularly, it could not cope with occlusion situations. The cooperative tracking approach presented in this article alleviates this by including smart device information. It can provide a precise VRU position even in the short absence of any visual information.

### III. METHOD

We envision to make use of data provided by all road users including infrastructure in the local environment, allowing to detect VRUs, classify, localize, and track them. Here, we restrict ourself to a research intersection [8] and smart devices carried by the cyclist. A schematic of our approach, which illustrates the components and their interaction, is depicted in Fig. 1. In the first stage, the cyclist and especially his head is detected in the camera images. On top of that, a 2D head tracking algorithm is presented to overcome minor detection misses and occlusions. Subsequently, the 3D head position is triangulated using the 2D head position of both camera images. Human activity recognition and machine learning techniques [9] based on the smart device inertial measurement unit (IMU) are used to estimate the cyclists yaw rate and velocity. These estimates are sent to the infrastructure, e.g., using an ad hoc network. The triangulated head position and velocity and yaw rate estimates are then combined using an extended Kalman filter implementing the cooperative tracking. We focus on tracking the head for two reasons: First, the head is a good indicator for human intentions [10], second, it is in plain view from different camera perspectives and, therefore, perfectly suited for triangulation. Moreover, the integration of smart device based velocity and yaw rate estimates allows to track a cyclist even in the absence of any visual information.

For the communication between the smart devices and the infrastructure, we assume that it is realized by means of an ad hoc network. The approach assumes an idealized communication medium without any considerable communication delays and synchronized devices using GPS timestamps.

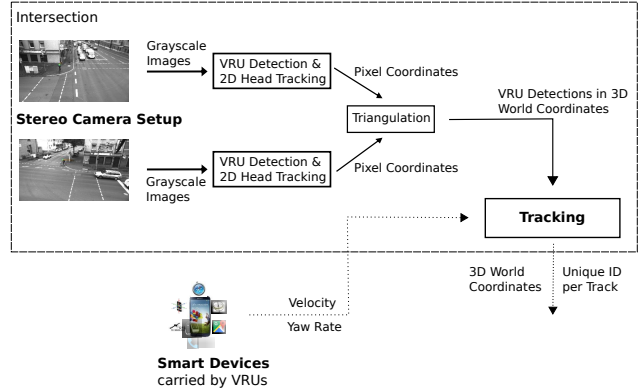


Fig. 1. VRU tracking based on infrastructure and smart devices.

Furthermore, we assume that the association between the smart device and the detected cyclist in the camera image is given.

#### A. Image based VRU Detection

A setup of two high definition cameras mounted in a wide stereo angle at opposite corners of the intersection forms one part of the cooperating agents. We perform image based cyclist detection on every camera. For previous works referenced in Sec. II we have already built up a dataset of labeled head positions of cyclists in sequences of images. The dataset consists of recorded scenarios with smart device equipped VRUs. To reduce the labeling effort, the head labeling was only done on the smart device equipped VRUs and not on all VRUs visible in the frames.

The detector development is performed with the state of the art TensorBox framework described in [11]. The framework enables, in a comfortable way, training of neural networks to detect objects in images using a classifier of ones choice embedded in the architecture described in [12]. As a classifier we use the default GoogLeNet [13]. The proposed architecture is, although a generic one, especially applicable to person detection in crowded scenes as it directly generates a set of object bounding boxes as an output and aims to make the post processing in form of merging and non-maximum suppression to avoid multiple detections obsolete.

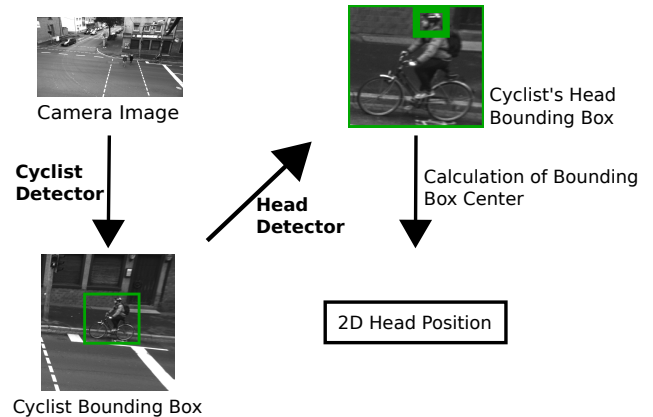


Fig. 2. Cyclist's head detection using self trained cyclist and head detectors.

As we are interested in tracking cyclists via the center of their heads, we trained two detectors. Fig. 2 illustrates

the detection process. At first, a cyclist detector is essential. TensorBox uses bounding box labels, but in our dataset only head positions are available. To overcome this gap, the bike detector proposed by Felzenszwalb et al. in [14] is applied to a sufficiently big region of interest around the labeled head position to receive a bounding box surrounding the bike. The final cyclist bounding box has the width and bottom line of the bike bounding box and the top line is placed half a head size above the labeled head position. For the head size a fixed value is assumed in combination with a lookup table to cope with the dependency from the objects distance to the camera. Every labeled frame available at the time of training and the corresponding calculated cyclist bounding boxes were used as training dataset. The resulting cyclist detector operates on camera images and produces bounding boxes as an output.

Having the bounding box surrounding a cyclist, we are still in need for the head position. Therefore, a head detector was trained in an analogue way. This time, only the calculated bounding box around the labeled cyclist was used as input image in combination with a bounding box surrounding the head, which was determined just as above. The training set consisted of every 50<sup>th</sup> of all available labeled frames. The trained detector performs on cyclist bounding boxes and produces bounding boxes surrounding the head of the cyclist. The output of the detection algorithm is a head position that is a simple determination of the center of the bounding box produced by the head detector.

In the end, a detection algorithm is given that provides the position in pixel coordinates of the heads of the cyclists appearing in a given camera image. In the rare cases of double detections, i.e., detections within a distance of 15 pixels, only the first detection is taken.

### B. Tracking in 2D Images

Due to changing weather and illumination situations or simply short (partly) occlusions detection misses are unavoidable. To reduce the number of such detection misses, a constant velocity (CV) Kalman filter (KF) [15] in combination with a memory functionality is implemented. The KF operates on the state space  $[u, v, \dot{u}, \dot{v}]$ , with  $u$  and  $v$  being pixel coordinates and  $\dot{u}$  and  $\dot{v}$  being the corresponding derivatives in time. The process noise matrix  $Q$  is determined as described in [15], the measurement noise matrix  $R$  via an ordinary parameter search.

In every frame each detection is tried to be assigned to a predicted position of an existing KF track. To solve the assignment problem, the Munkres algorithm [16] is used. Every track with an assigned detection gets updated by it. If there is a detection with no track assigned, because it is more than 40 pixels in Euclidean distance away from every existing track, a new KF track is started. If there is a track with no detection assigned, an internal detection miss counter is increased. If the ratio of the miss counter to the total age of the track exceeds 30%, the track is considered lost and gets deleted. A track is also considered lost, when there has not been an update for one second. To make the system more robust, a track has to have at least an age of four frames to be

considered as valid. This introduces some delay, but reduces the number of false positives.

The output of the combined 2D detection and tracking is a number of tracks. The current position in pixel coordinates of each track is interpreted as detection and considered in the following triangulation.

### C. Triangulation of VRU Detections

The wide angle setup of the cameras at the intersection allows for determination of 3D coordinates via triangulation. It is designed for a spatial resolution better than 10 cm [8]. The calculation of triangulation follows the basic knowledge of epipolar geometry as it can be found in [17]. The interesting thing about triangulation in our setting is that it can also be used to determine false positive (FP) detections. If there is a detection in one camera, but no such on the corresponding epipolar line in the other camera, then the first detection might be a FP. It, of course, might also be possible that on the second camera the detection is simply missing due to occlusion or a false negative. Nevertheless, if there are two detections in the two cameras corresponding to one 3D point, it is a strong indicator for a true detection. The triangulation not only produces 3D coordinates that can be shared with other entities in the intersection, it also contributes to a more reliable VRU detection.

### D. Yaw Rate and Velocity Estimation using Smart Devices

In this section the yaw rate and velocity estimation using smart devices is described. Besides an IMU also position and velocity information by the Global Navigation Satellite Systems (GNSS) is nowadays available on nearly every smart device. GNSS requires the availability of satellite signals, which is especially in urban areas not always given or noisy due to multipath effects. For these reasons our approach only considers inertial measurements, i.e., the accelerometer and gyroscope sensor.

Inertial navigation systems (INS) [18] are widely used in aerospace and automotive industry, e.g., for dead reckoning. Here, first the attitude is estimated and then subsequently the velocity and position is obtained by integration. These algorithms are not directly applicable for smart devices carried by pedestrians and cyclists as small errors in the attitude calculation, due to relative high ego motion, e.g., cyclists pedalling, and low-cost inertial sensors, accumulate, deteriorating the velocity or position estimation. In order to be more robust against errors in the attitude estimation, our approach for velocity estimation is realized by means of human activity recognition techniques [9]. A schematic of the approach is depicted in Fig. 3.

The yaw rate  $\dot{\gamma}$  and velocity  $v$  are measured in the local tangential frame  $t$ , i.e., an arbitrary local coordinate frame whose  $z$ -axis points toward the sky and is perpendicular to the local ground plane. The velocity  $v$  is defined as the magnitude of the velocity  $v_x$  and  $v_y$  in the local tangential frame. We assume that the cyclist is always moving in forward direction and ego-motion resulting in an increased velocity magnitude, e.g., small side steps are negligible. By

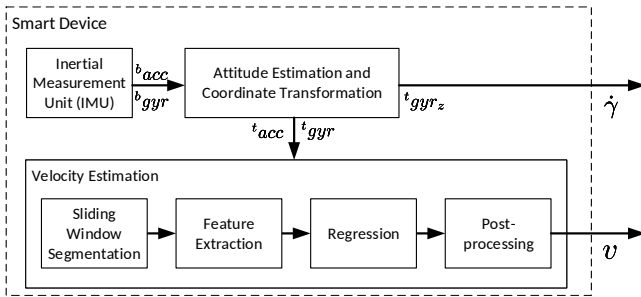


Fig. 3. Process of smart device based yaw rate and velocity estimation. The upper blocks include the attitude estimation used for transformation of the measurements into the local tangential frame. The lower block depicts the human activity pipeline used for velocity estimation.

considering only the magnitude of the velocity and the yaw rate (i.e., angular velocity around the  $z$ -axis), there is no need to estimate the transformation of the device with respect to a global coordinate frame. Moreover, we do not need a compass which is sensitive to a precise calibration [19].

The acceleration  $b_{acc}$  and gyroscope  $b_{gyr}$  measurements are obtained in the body coordinate frame  $b$ . The transformation between  $b$  and the local tangential plane  $t$ , i.e.  $b_{acc}$  and  $b_{gyr}$  to  $t_{acc}$  and  $t_{gyr_z}$ , is obtained by estimating the local gravity vector, which is supplied by nearly all modern mobile systems. We therefore assume this transformation as given. The approach presented here uses features computed from accelerometer and gyroscope sensors sampled with a frequency of 100 Hz.

We assume that the ego-motion of the smart device and the cyclists with respect to the rotation around the  $z$ -axis of the local tangential frame is negligible. Then  $t_{gyr_z}$ , i.e., rotation around the  $z$ -axis, corresponds to the yaw rate  $\dot{\gamma}$ .

The velocity estimation is realized by a machine learning approach based on  $t_{acc}$  and  $t_{gyr_z}$ . Orientation-independence is achieved by considering the magnitude of the accelerometer and gyroscope values in the local horizontal  $x - y$  plane. Moreover, the projection of the sensor values on the local vertical  $z$ -axis, i.e., the gravity axis, is considered. A sliding window segmentation of window sizes 1 s is performed on each of the transformed signals and features, such as the mean and energy, are computed. These features are used, since calculating for example the mean of the acceleration is directly related to the velocity. Additionally, the magnitude of the discrete Fourier transform (DFT) coefficients are also considered as input features, as successfully applied for human walking speed estimation in [20]. The coefficients are normalized with respect to the overall energy in the respective window. As in [20], the window size is set to 5.12 s and coefficients up the 30<sup>th</sup> order are considered.

The velocity estimation is realized by means of a frame-based extreme gradient boosting regression [21] at discrete points with a frequency of 50 Hz. The regression model is trained with sample velocity data originating from manually labeled and additionally smoothed head trajectories. Finally, the velocity gradient boosting regression's prediction is smoothed with a moving average filter of window size 0.25 s.

### E. Cooperative Tracking

So far, we've presented, how we attain the 3D coordinate positions of cyclists moving in the field of view of the cameras installed at the intersections and how we extract velocity and yaw rate data from the smart devices of the observed cyclists. To combine velocity, yaw rate and 3D coordinate positions, we set up an extended Kalman filter (EKF) [15] with the state space  $[x, y, z, \dot{z}, \gamma, \dot{\gamma}, v]$  with  $x, y, z$  being the three coordinates describing the position of the cyclist,  $\dot{z}$  the derivative of  $z$  in time,  $\gamma$  the yaw,  $\dot{\gamma}$  the yaw rate and  $v$  the absolute velocity. The corresponding time  $T$  dependent state transition matrix is given by

$$\begin{bmatrix} x + \cos(\gamma) a - \sin(\gamma) b \\ y + \sin(\gamma) a + \cos(\gamma) b \\ z + \dot{z}T \\ \dot{z} \\ \gamma + \dot{\gamma}T \\ \dot{\gamma} \\ v \end{bmatrix}$$

with  $a = \frac{\sin(\dot{\gamma}T)v}{\dot{\gamma}}$  and  $b = \frac{(1-\cos(\dot{\gamma}T))v}{\dot{\gamma}}$ . The motion model is the bike model adapted from the work by Bar-Shalom and Kirubarajan [15]. To linearize the non-linear model, the EKF uses the *Jacobian* of the state transition matrix. The time difference between two measurements is 20 ms. The standard deviations of the state vector were chosen as  $\sigma := [0.1, 0.1, 0.1, 0.02, 0.04, 0.075, 0.075]$  by analyzing the given data and keeping in mind that most of the change of state variable  $i$  from one time stamp to the next one should be explained within  $3\sigma_i$ . The units are m for positional variables and rad for angular variables. The process noise matrix  $Q$  was chosen as a diagonal matrix with  $\sigma \cdot \sigma$  on its diagonal under the simplifying assumption that the variables are uncorrelated.

We consider three measurement models. The first one performs an update with both the 3D position and the smart device data, the second one with the smart device data only, and the third one with 3D position only. This covers all possible states of information per time stamp. If there is no information at a time stamp, no update can be done. The standard deviations for the measurement noise are given by 0.2 m for  $x, y$  and  $z$ , 0.1  $\text{rad s}^{-1}$  for  $\dot{\gamma}$  and 0.8  $\text{m s}^{-1}$  for  $v$ . They were estimated by comparison with the ground truth data.

Following the idea of the already presented 2D tracking, we want to overcome situations of missing data by a memory functionality. The same algorithm as in Sec. III-B is also used in the 3D scenario with the following differences in parameters. If a detection is more than 2 m away from a track, it is not considered for an assignment in the Munkres algorithm anymore. A track is lost, when there has not been an update in position for more than 2 s or the miss ratio exceeds 50%. The assignment of the smart device data to the corresponding positional track is not considered. Therefore, the track with the smart device equipped cyclist gets updated with smart device data every frame it is available.

## IV. DATA ACQUISITION AND EVALUATION

### A. Data Acquisition

The developed tracking algorithm is evaluated in experiments conducted with 52 female and male test subjects in the age between 18 - 54. The test subjects were equipped with a Samsung Galaxy S6 smart device carried in the trouser front pocket and instructed to move between certain points at an intersection while following the traffic rules. The recorded scenes included waiting, starting, driving through, and turning (left, right) behavior. To record the cyclist trajectories, a wide angle stereo camera system consisting of two high definition cameras ( $1920 \times 1080$  px, 50 fps) [8] was used. The timestamps of the smartphone and the research intersection are synchronized offline. The head tracks on the video cameras are labeled by human operators and assumed to be close to the ground truth. The labeled positions are triangulated to obtain 3D coordinates.

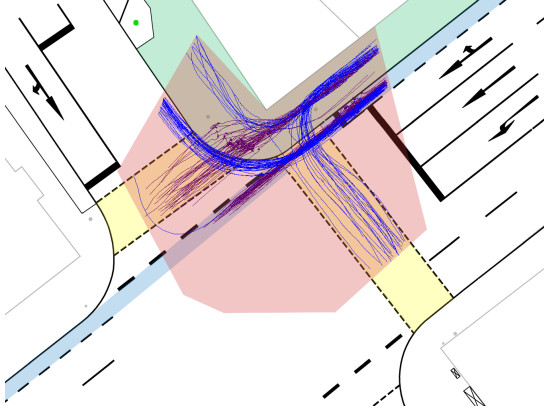


Fig. 4. Overview of the intersection with all cyclists' trajectories. The turning right tracks are blue, whereas the starting ones are purple.

### B. Evaluation

In total 74 turning right and 87 starting scenes are fully labeled, processed, synchronized and thus available for evaluation. The extracted trajectories are plotted in Fig. 4. Blue ones represent the turning right scenarios, whereas purple ones visualize the starting scenes. The intersecting field of view of both cameras is sketched in light red. Starting scenes are designed in such a way that the test subjects approach red traffic lights. They have to stop and start in a straight direction, when the lights turn green again. This should ensure a natural starting behavior. For the evaluation, only the process after the stopping at the red lights is considered. In the case of turning right, the test subject may as well stop at red lights before turning right or be in motion throughout the complete scene. To cut off the waiting, only the last 12 s of a scene were used.

The use case of our cooperative approach are scenes, where occlusions compromise a proper tracking of cyclists. If the 2D position information by one camera is missing, there is no triangulation possible anymore. Therefore, there is no 3D position as well. We create artificial occlusions of 1 s and 2 s duration by dropping detections in one camera.

Occlusions in accelerating or direction changing motions are the most interesting, because they hide crucial information for tracking. We thus aim to place the artificial occlusions in such states. The recorded scenes end shortly after performing starting or turning, as the cyclists leave the camera view without stopping. Therefore, the occlusions were defined in a fixed temporal distance to the last frame. The 1 s occlusion starts at the same frame like the 2 s one.

We will compare the trajectories created by the intersection only model with the ones by the smart device integrating model. In the field of object tracking the MOTP and MOTA metrics are established. In [22], they are defined for the multi-object tracking scenario. In our setting we only have one ground truth trajectory per scene. Therefore, we define MOTP and MOTA for the 3D single object tracking task

$$\text{MOTP} = \frac{\sum_t d_t}{\sum_t c_t} \quad (1)$$

$$\text{MOTA} = 1 - \frac{\sum_t (dm_t + 2 * lm_t)}{\sum_t g_t} \quad (2)$$

with  $d_t$  being the Euclidean distance of the modeled track to the ground truth track at time  $t$ ,  $c_t$  being 1 at time  $t$ , if  $d_t$  is smaller than a defined threshold  $\tau$  and 0 otherwise. If  $c_t$  equals 0, it is called a miss and the summand at time  $t$  for MOTP is zero. The variable  $g_t$  defines the number of ground truth labels at time  $t$ . The variable  $dm_t$  counts the number of misses at time  $t$  due to a missing track, i.e., a detection miss, whereas  $lm_t$  counts the number of misses due to a distance  $d_t$  bigger than  $\tau$ , i.e., a localization miss.

MOTP is used to measure how accurately a track follows the ground truth, if a track exists. MOTA penalizes missing tracks. Both have to be considered to assess the quality of a track. At the same time, minor differences in MOTP or MOTA do not indicate a significantly better or worse track. Therefore, the significance thresholds  $\alpha$  for MOTA and  $\beta$  for MOTP are introduced and track  $A$  is considered *better performing* than track  $B$ , if the condition

$$(\text{MOTA}_A > \text{MOTA}_B + \alpha) \wedge (\text{MOTP}_A < \text{MOTP}_B + \beta) \quad (3)$$

or the condition

$$(\text{MOTA}_A > \text{MOTA}_B - \alpha) \wedge (\text{MOTP}_A < \text{MOTP}_B - \beta) \quad (4)$$

holds. We define the metric

$$\text{MOTAP}_{\alpha,\beta}(A, B) := \begin{cases} 1, & \text{if condition 3 or 4 holds} \\ 0, & \text{otherwise} \end{cases}$$

to be able to rank the performance of two tracks compared to the ground truth.

## V. EXPERIMENTAL RESULTS

In this section we compare the position only tracking model, referred  $\mathcal{P}$ , with the one combining positional and smart device data, referred  $\mathcal{C}$ . We evaluate in several test runs on both starting and turning right scenes the ability of the specific tracking models to follow the ground truth track.

Tab. I presents MOTP, given in mm, and MOTA for the miss threshold  $\tau = 1$  m and no artificial occlusion using the characteristic numbers minimum, maximum and mean. MOTAP is calculated with  $\alpha = 0.025$  and  $\beta = 10$ .

The choice of  $\tau = 1$  m, meaning a miss is counted, if the distance of a track to the ground truth exceeds 1 m, is quite a standard choice in 3D tracking [23]. The value for  $\alpha$  is intended to be a small threshold and  $\beta$  is intentionally quite high relative to the mean performance. The reason is that a track with a better MOTA score can have a worse MOTP score following the ground truth roughly, than a track quickly surpassing the  $\tau$  threshold. Nevertheless, the behavior of the former track should be rated better. The choice of  $\beta$ , therefore, lays more weight on MOTA.

TABLE I  
EVALUATION OF ALL SCENES WITHOUT OCCLUSIONS.

| Scenes   | MOTP <sub><math>\mathcal{P}</math></sub> |            |             | MOTA <sub><math>\mathcal{P}</math></sub> |            |             | MOTAP( $\mathcal{P}, \mathcal{C}$ ) |
|----------|--|------------|-------------|--|------------|-------------|-------------------------------------|
|          | <i>max</i>                               | <i>min</i> | <i>mean</i> | <i>max</i>                               | <i>min</i> | <i>mean</i> | $\Sigma$                            |
| Starting | 182                                      | 31         | 78          | 1  | 0.206      | 0.976       | 8                                   |
| Turning  | 229                                      | 43         | 95          | 1  | 0.273      | 0.913       | 9                                   |
| Scenes   | MOTP <sub><math>\mathcal{C}</math></sub> |            |             | MOTA <sub><math>\mathcal{C}</math></sub> |            |             | MOTAP( $\mathcal{C}, \mathcal{P}$ ) |
|          | <i>max</i>                               | <i>min</i> | <i>mean</i> | <i>max</i>                               | <i>min</i> | <i>mean</i> | $\Sigma$                            |
| Starting | 164                                      | 29         | 76          | 1  | 0.206      | 0.981       | 18                                  |
| Turning  | 187                                      | 41         | 89          | 1  | 0.290      | 0.930       | 30                                  |

One can see, that for both data sets, the models perform with an average accuracy of about 10 cm and an average MOTA score above 90% without any artificial occlusions. The turning scenes are more challenging, as both MOTA and MOTP scores are worse in average. The two models operate on a comparable performance regarding the mean values of MOTP and MOTA, but looking at the scene wise comparison via MOTAP, combining MOTA and MOTP, one can see that model  $\mathcal{C}$  outperforms model  $\mathcal{P}$ . Regarding the starting scenes, there are 8 scenes in which  $\mathcal{P}$  performs better than  $\mathcal{C}$ , but 18 vice versa. Considering the turning scenes, the difference is even greater.

TABLE II  
MOTAP OF SCENES WITH LESS THAN 30 MISSING DETECTIONS.

| Scene Type | #Scenes | $\Sigma$ MOTAP( $\mathcal{P}, \mathcal{C}$ ) | $\Sigma$ MOTAP( $\mathcal{C}, \mathcal{P}$ ) |
|------------|---------|--|--|
| Starting   | 46      | 4  | 3  |
| Turning    | 42      | 5  | 15   |

Although, there are no artificial occlusions in the scenes evaluated in Tab. I there are frames with no detections due to detector failures or natural occlusions. To compare the two models on scenes with a high detection rate, in Tab. II only scenes with less than 30 missing detections are considered. This leads to an evaluation on roughly the half of all scenes with model  $\mathcal{P}$  performing slightly better than model  $\mathcal{C}$  in the waiting scenes, but still worse in the starting scenes. This gives a first indication that when it comes to more challenging scenarios or detection dropouts, the additional smart device data adds to a more robust and accurate system.

The scenes evaluated in Tab. III contain the artificial occlusions defined in Sec. IV-B in addition to the natural detection misses. Focusing on the starting scenes, the fused model outperforms the position only model by far. There are 9 scenes with model  $\mathcal{P}$  producing a better track than  $\mathcal{C}$ , but

TABLE III  
MOTAP OF SCENES UNDER ARTIFICIAL OCCLUSIONS.

| Scene Type | Occlusion[s] | $\Sigma$ MOTAP( $\mathcal{P}, \mathcal{C}$ ) | $\Sigma$ MOTAP( $\mathcal{C}, \mathcal{P}$ ) |
|------------|--------------|--|--|
| Starting   | 1            | 9  | 39   |
| Starting   | 2            | 10   | 39   |
| Turning    | 1            | 7  | 41   |
| Turning    | 2            | 2  | 26   |

39 the other way around. The velocity information by the smart devices helps to cope with the acceleration the cyclist is performing. Considering two seconds of occlusion, the difference in MOTAP is almost the same. There are 7 turning scenes under a 1 s occlusion with model  $\mathcal{P}$  performing better than  $\mathcal{C}$  against 41 vice versa. The same domination of model  $\mathcal{C}$  does not stand for the turning scenarios under a 2 s occlusion, as only 26 scenes show a better performance according to MOTAP. It seems, that over a longer time the gain of the yaw rate and velocity information decreases in the more complex turning scenes.

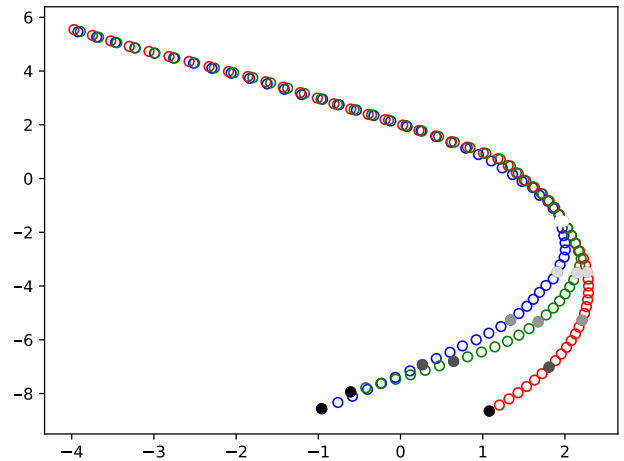


Fig. 5. Example of a turning right scenario under a 2 s occlusion with model  $\mathcal{C}$  (green) following the ground truth trajectory (blue) closely in contrast to model  $\mathcal{P}$  (red).

Fig. 5 shows an example scene for turning right with a 2 s occlusion. For visibility reasons only every 4<sup>th</sup> frame in  $x$ - and  $y$ -direction is plotted. The coordinate system is the local one at the intersection and the units are given in meters. A circle represents a single position in a track. Blue represents the ground truth, green the model  $\mathcal{C}$  and red the model  $\mathcal{P}$  track. The filled circles of a single gray-scale tone mark the positions of the three tracks at the same timestamp to visualize velocity differences. The white filled circles mark the start of the occlusion. The green track follows the ground truth closely, but looking at the synchronization points, it slightly falls back. Considering the visualizations like in Fig. 5 for all turning right scenes, the velocity estimates received by the smart devices tend to have a delay when it comes to acceleration. Still, the combined model manages to track the cyclist quite accurate despite the occlusion. The intersection only model is unable to do so.

In Fig. 6 an example is shown with model  $\mathcal{C}$  drifting apart from the ground truth track. A strong velocity underestimation and an imprecise yaw rate data lead to the drift. As model  $\mathcal{C}$  is under occlusion purely relying on smart device



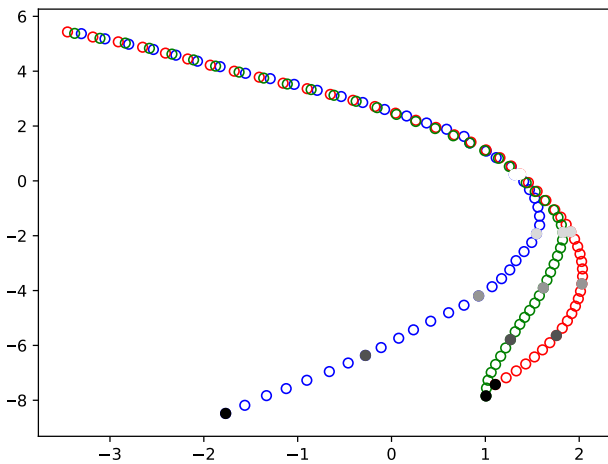


Fig. 6. Example of a turning right scenario under a 2 s occlusion with model  $\mathcal{C}$  (green) failing to follow the ground truth track (blue) closely.

data, it is sensible to imprecise data. Nevertheless, only in rare cases this leads to a worse performance than considering no additional information at all. Tab. III shows the great gain of our approach. There is potential left in the quality of the smart device data. Using the ground truth velocity instead of the measured one would reduce the number of scenes with model  $\mathcal{P}$  performing better than model  $\mathcal{C}$  to one in any case of Tab. III.

## VI. CONCLUSIONS AND FUTURE WORK

In this article, we presented an approach to cooperatively track cyclists. The cooperation combined smart device information with an infrastructure based detection to improve the infrastructure only tracking of cyclists. We showed by evaluation of real traffic starting and turning right scenarios using MOTA, MOTP, and the novel MOTAP measure that the addition of smart device information leads to a better tracking of cyclists in terms of accuracy and robustness. We assumed an ideal communication medium with negligible delay, but operated with real smart device sensor data.

Our future work will focus on the improvement of the accuracy of smart device data. Especially the velocity estimation holds room for improvements. This article concentrated on the use of smart device data. In a next step, we will transfer infrastructure information to smart devices to improve the self-localization methods of smart devices via intersection data. To be able to evaluate the gain of our approach with as few simplifying assumptions as possible, we will tackle the problem of associating smart devices to infrastructure based detections and a realistic communication medium in further research, getting us closer towards our envisioned future traffic scenario [1].

## VII. ACKNOWLEDGMENT

This work results from the project DeCoInt<sup>2</sup>, supported by the German Research Foundation (DFG) within the priority program SPP 1835: "Kooperativ interagierende Automobile", grant numbers DO 1186/1-1, FU 1005/1-1, and SI 674/11-1. Additionally, the work is supported by Zentrum Digitalisierung Bayern.

## REFERENCES

- [1] M. Bieshaar, G. Reitberger, S. Zernetsch, B. Sick, E. Fuchs, and K. Doll, "Detecting intentions of vulnerable road users based on collective intelligence," in *AAET Automatisiertes und vernetztes Fahren*, Braunschweig, Germany, 2017, pp. 67–87.
- [2] M. Bieshaar, S. Zernetsch, M. Depping, B. Sick, and K. Doll, "Cooperative starting intention detection of cyclists based on smart devices and infrastructure," in *ITSC*, Yokohama, Japan, 2017.
- [3] "Ko-FAS: Cooperative Sensor Systems and Cooperative Perception Systems for Preventive Road Safety," 2013, Internet: <http://www.kofas.de>, [Jan. 09, 2018].
- [4] D. Thielen, T. Lorenz, M. Hannibal, F. Koster, and J. Plattner, "A feasibility study on a cooperative safety application for cyclists crossing intersections," in *ITSC*, Anchorage, AK, 2012, pp. 1197–1204.
- [5] S. Engel, C. Kratzsch, K. David, and M. Warkow, D. und Holzknecht, "Car2pedestrian positioning: Methods for improving gps positioning in radio-based vru protection systems," in *6. Tagung Fahrerassistenzsysteme*, Munich, Germany, 2013.
- [6] T. Ruß, J. Krause, and R. Schönrock, "V2x-based cooperative protection system for vulnerable road users and its impact on traffic," in *ITS World Congress*, 2016.
- [7] P. Merdrignac, O. Shagdar, and F. Nashashibi, "Fusion of perception and v2p communication systems for safety of vulnerable road users," *Transactions on Intelligent Transportation Systems*, vol. 18, no. 7, pp. 1740–1751, 2016.
- [8] M. Goldhammer, E. Strigel, D. Meissner, U. Brunsmann, K. Doll, and K. Dietmayer, "Cooperative multi sensor network for traffic safety applications at intersections," in *IEEE International Conference on Intelligent Transportation Systems (ITSC)*, Anchorage, AK, 2012, pp. 1178–1183.
- [9] A. Bulling, U. Blanke, and B. Schiele, "A tutorial on human activity recognition using body-worn inertial sensors," *ACM Computing Surveys*, vol. 46, no. 3, pp. 1–33, 2014.
- [10] A. Hubert, S. Zernetsch, K. Doll, and B. Sick, "Cyclists' starting behavior at intersections," in *IV*, Los Angeles, CA, 2017, pp. 1071–1077.
- [11] "Tensorbox," 2016, Internet: <https://github.com/Russell91/TensorBox>, [Jan. 12, 2018].
- [12] R. Stewart and M. Andriluka, "End-to-end people detection in crowded scenes," *CoRR*, vol. abs/1506.04878, 2015. [Online]. Available: <http://arxiv.org/abs/1506.04878>
- [13] C. Szegedy, W. Liu, Y. Jia, P. Sermanet, S. E. Reed, D. Anguelov, D. Erhan, V. Vanhoucke, and A. Rabinovich, "Going deeper with convolutions," *CoRR*, vol. abs/1409.4842, 2014. [Online]. Available: <http://arxiv.org/abs/1409.4842>
- [14] P. F. Felzenszwalb, R. B. Girshick, D. McAllester, and D. Ramanan, "Object detection with discriminatively trained part-based models," *TPAMI*, vol. 32, no. 9, pp. 1627–1645, Sept 2010.
- [15] Y. Bar-Shalom, X. R. Li, and T. Kirubarajan, *Estimation with Applications to Tracking and Navigation: Theory Algorithms and Software*. John Wiley and Sons, 2001.
- [16] J. Munkres, "Algorithms for the assignment and transportation problems," *Journal of the Society for Industrial and Applied Mathematics*, vol. 5, no. 1, pp. 32–38, March 1957.
- [17] R. Hartley and A. Zisserman, *Multiple View Geometry in Computer Vision*, 2nd ed. New York, NY, USA: Cambridge University Press, 2003.
- [18] D. Titterton and J. Weston, *Strapdown Inertial Navigation Technology*. Reston, VI: The Institution of Electrical Engineers, 2004.
- [19] T. Michel, P. Genevès, H. Fourati, and N. Layaïda, "On Attitude Estimation with Smartphones," in *PerCom*, Kona, HI, 2017.
- [20] J. Park, A. Patel, D. Curtis, S. Teller, and J. Ledlie, "Online pose classification and walking speed estimation using handheld devices," in *UbiComp*, New York, NY, 2012, pp. 113–122.
- [21] T. Chen and C. Guestrin, "Xgboost: A scalable tree boosting system," in *KDD16*, San Francisco, CA, 2016, pp. 785–794.
- [22] K. Bernardin and R. Stiefelhagen, "Evaluating multiple object tracking performance: The clear mot metrics," *EURASIP Journal on Image and Video Processing*, vol. 2008, no. 1, pp. 246–309, May 2008.
- [23] A. Milan, K. Schindler, and S. Roth, "Challenges of ground truth evaluation of multi-target tracking," in *2013 IEEE Conference on Computer Vision and Pattern Recognition Workshops*, 2013, pp. 735–742.